

Update on Multiparametric MRI of Urinary Bladder Cancer

Christian B. van der Pol, MD,¹ Andrew Chung, MD,² Christopher Lim, MD,³
Niket Gandhi, MD,⁴ Wendy Tu, MD,⁴ Matthew D.F. McInnes, MD,⁴ and
Nicola Schieda, MD^{4*}

While many institutions perform MRI during the work-up of urinary bladder cancer, others use MRI rarely if at all, possibly due to a variation in the reported staging accuracy and unfamiliarity with the potential benefits of performing MRI. Through increased application of functional imaging techniques including diffusion-weighted imaging (DWI) and dynamic contrast-enhanced (DCE) imaging, there has been a resurgence of interest regarding evaluation of bladder cancer with MRI. Several recent meta-analyses have shown that MRI is accurate at differentiating between $\leq T1$ and $T2$ disease (with pooled sensitivity/specificity of $\sim 90/80\%$) and differentiating between $T2$ and $\geq T3$ disease. DWI and DCE, in combination with high-resolution T_2 -weighted images, improves detection and possibly local staging accuracy of bladder cancer. High b value echo-planar DWI is particularly valuable for tumor detection. Zoomed field of view and segmented readout DWI techniques improve image quality by reducing susceptibility artifact, while methods to extract calculated high b value images save time and improve the contrast-to-noise ratio. DCE traditionally required imaging of the pelvis with high temporal but lower spatial resolution; however, advances in parallel and keyhole imaging techniques can preserve spatial resolution. The use of compressed sensing reconstruction may improve utilization of DCE of the bladder, especially when imaging the abdomen simultaneously, as in MR urography. Quantitative imaging analysis of bladder cancer using pharmacokinetic modeling of DCE, apparent diffusion coefficient values, and texture analysis may enable radiomic assessment of bladder cancer grade and stage.

Level of Evidence: 3

Technical Efficacy: Stage 2

J. MAGN. RESON. IMAGING 2018;48:882–896.

The American Cancer Society estimates that there will be 81,190 new cases of urinary bladder cancer, and 17,240 deaths from bladder cancer, in the United States in 2018.¹ Bladder cancer is the sixth most common type of cancer.¹ The management of bladder cancer is determined predominantly by stage and grade of disease at diagnosis. Local staging is traditionally dependent on findings at cystoscopy and transurethral resection of bladder tumor (TURBT). Abdomen pelvis computed tomography (CT) is commonly used to assess for nodal disease or metastases, along with either a preoperative chest x-ray or chest CT.² Fluorodeoxyglucose positron emission tomography CT (FDG PET/CT) can improve sensitivity for detection of nodal and metastatic disease and may be appropriate in some settings.^{3,4}

A key distinction for the local staging of bladder cancer is the presence or absence of muscle invasion, which has a significant impact on the management strategy as outlined in multiple guidelines including those issued by the National Comprehensive Cancer Network (NCCN), the American Urological Association/Society of Urologic Oncology (AUA/SUO), and the European Association of Urology (EAU).^{5–7} Muscle-invasive bladder cancer (MIBC) is treated with radical cystectomy and increasingly neoadjuvant therapy. Non-MIBC is often treated with bladder-sparing techniques. TURBT is the current standard for determining the presence or absence of muscle invasion, and also provides an estimate of histologic subtype and grade, and in some instances can be

View this article online at wileyonlinelibrary.com. DOI: 10.1002/jmri.26294

Received May 23, 2018, Accepted for publication Jul 5, 2018.

*Address reprint requests to: N.S., The Ottawa Hospital, 1053 Carling Avenue, Ottawa, ON, K1Y 4E9, Canada. E-mail: nschieda@toh.on.ca

From the ¹Department of Radiology, Juravinski Hospital and Cancer Centre, HHS, McMaster University, Hamilton, ON, Canada; ²Department of Radiology, Beth Israel Deaconess Medical Center, Harvard Medical School, Boston, Massachusetts, USA; ³Division of Abdominal Imaging and Intervention, Department of Radiology, Brigham and Women's Hospital, Harvard Medical School, Boston, Massachusetts, USA; and ⁴Department of Radiology, The Ottawa Hospital, University of Ottawa, Ottawa, ON, Canada

completely curative if the entire tumor is resected.⁸ However, TURBT has been found to underestimate T stage in up to 40% of patients, is inaccurate at determining tumor grade in up to 15% of patients, and frequently needs to be repeated.^{9,10} Furthermore, adherence to guidelines recommending repeat TURBT varies widely between urologists.¹¹

Multiparametric magnetic resonance imaging (mp-MRI) of the bladder has reemerged as a noninvasive tool that can help assess the local stage and grade of bladder cancer with relatively high accuracy.^{12–17} mp-MRI consists of high-resolution T₂-weighted (T₂W) images, diffusion-weighted imaging (DWI), and dynamic contrast-enhanced (DCE) imaging.¹⁶ mp-MRI can demonstrate tumor growth into the bladder detrusor muscle, peri-vesical extension, and can also assess regional nodes and pelvic metastases. mp-MRI remains relatively accurate at bladder cancer local staging even after TURBT.¹⁸ It is anticipated that utilization of mp-MRI for bladder cancer local staging will increase as awareness of its accuracy in the urology community improves. Several recent meta-analyses assessing the topic of local staging of bladder cancer with mp-MRI confirm an increased interest in the genitourinary community.^{19–21}

This article reviews urinary bladder anatomy and histology with MRI correlations, MRI techniques including updates on DWI, DCE, and MR urography (MRU), MRI staging and accuracy, bladder cancer variants, and finally discusses the applications of radiomic analysis and machine learning to bladder cancer.

Bladder Anatomy

The luminal surface of the bladder is lined by the urothelium, an epithelial layer which is intermediate between nonkeratinizing squamous and pseudostratified columnar epithelium and 3–7 cells thick depending on the degree of bladder distention. The urothelium is the most superficial layer of the bladder wall mucosa, which is composed of the urothelium, the loose connective tissue of the lamina propria (containing blood vessels, lymphatics, and fat), and an incomplete and poorly-developed muscle layer known as the muscularis

mucosa.²² Deep to the mucosa lies the muscularis propria, also known as the detrusor muscle, which is composed of layers of smooth muscle (inner longitudinal, middle circular, and outer longitudinal) as well as interspersed paraganglia.²³ The detrusor muscle provides the primary contractile function for the bladder. A loose connective tissue layer of adventitia surrounds the muscularis propria.

Several bladder anatomic structures can be identified and assessed on both MRI and cystoscopy, and may serve as useful landmarks when describing pathology. This includes the ureteric orifices and the interureteric ridge, which extends between the ureteric orifices. Together with the internal urinary meatus, these structures define the bladder trigone.

At MRI, the bladder wall typically demonstrates uniformly low T₂W signal intensity, corresponding to the detrusor muscle, which is the only layer of the bladder wall that is readily depicted on noncontrast MRI.²⁴ Occasionally, an inner low T₂W signal intensity stripe and outer intermediate T₂W signal intensity stripe can be distinguished, corresponding to compact inner and loose outer smooth muscle layers, respectively.²⁵ At DCE imaging, the mucosa enhances early, with the detrusor muscle enhancing later. On delayed phase postcontrast T₁-weighted (T₁W) images, the bladder wall demonstrates homogeneous enhancement.²⁴

MRI Technique

The cornerstone for an MRI protocol that assesses the bladder is multiplanar high-resolution T₂W images. T₂W-MRI provides the best method to directly assess for depth of involvement of malignancies (which are typically of intermediate T₂W signal intensity) with respect to the low T₂W signal intensity detrusor muscle,^{24,26} which is a critical determinant of patient care in bladder malignancy (Fig. 1). T₂W imaging is generally performed using 2D fast or turbo spin-echo (FSE/TSE), which provide a robust signal-to-noise ratio (SNR) that is utilized to improve spatial resolution. Imaging can be performed at 1.5 or 3T, with improvements in SNR at 3T used to enhance spatial resolution. 3D FSE/TSE sequences (CUBE, General Electric

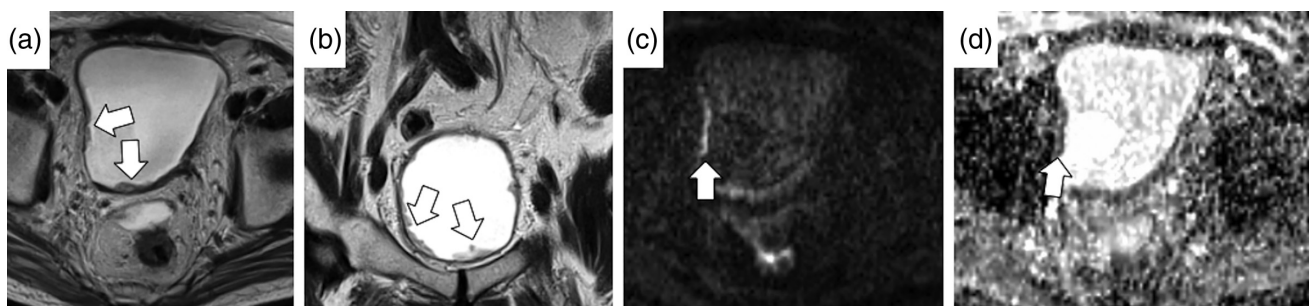


FIGURE 1: Multifocal urothelial carcinoma. a,b: Axial T₂W images at different levels reveal multiple intraluminal filling defects extending along the bladder wall with intermediate T₂W signal, without disruption of the underlying T₂ hypointense detrusor muscle, consistent with superficial spread of tumor (arrows). Axial $b = 1000 \text{ sec/mm}^2$ DWI (c) and corresponding ADC map (d) in the same patient show flat tumor that restricts diffusion. These findings are consistent with stage T1 disease.

[GE] Healthcare, Milwaukee, WI; SPACE, Siemens Healthcare, Erlangen, Germany; VISTA, Philips Healthcare, Best, Netherlands) can be used as an alternative to multiplanar 2D imaging; however, advantages of 3D imaging such as slight reductions in acquisition time, higher SNR, in-plane resolution, and the ability to generate oblique or off-axis reconstructions^{27–29} do not, in our opinion, improve assessment of the bladder compared to conventional 2D FSE/TSE, which in our own experience radiologists generally still prefer. Moreover, susceptibility to motion artifact during the 3D acquisition, which impacts the entire dataset, is a major limitation when imaging the bladder, which may be more impacted by the abdominal wall and bowel peristalsis than other deep pelvic structures such as the prostate and cervix. Patients should be instructed to partially void the bladder prior to pelvic MRI if overly full, as patients should be as comfortable as possible during the examination to prevent motion artifacts; however, a completely collapsed urinary bladder is not ideal, as a moderate amount of urine generally improves visualization of tumors and their relationship to the bladder wall. A bowel relaxant (hyoscine butylbromide [Buscopan] or glucagon) can be used to reduce artifacts related to bowel peristalsis in pelvic MRI; however, in our opinion it is generally not needed for high-quality bladder MRI, and at our institutions is not performed.³⁰ Bowel and abdominal wall motion can be mitigated wholly or in part by setting the phase-encoding direction to direct motion away from the bladder (eg, on an axial T₂W image, the phase-encoding direction should be set left-to-right rather than anterior-to-posterior) and by increasing the number of excitations (NEX). T₂W imaging can be acquired using periodically rotating overlapping parallel lines (PROPELLER, GE Healthcare; BLADE, Siemens Healthcare; MultiVane, Philips Healthcare), which has been shown to potentially improve image sharpness, overall image quality, and reduce artifact compared to conventional rectilinear filling of *k*-space in FSE/TSE,^{31,32} although at the cost of lower contrast.³³ We consider the choice of using conventional FSE/TSE versus periodically rotating overlapping parallel lines sequences an institutional preference; however, in cases of severe motion artifact on FSE/TSE, periodically rotating overlapping parallel lines sequence T₂W can be utilized as a backup to attempt to salvage an exam. Half-Fourier single-shot FSE/TSE (ssFSE, GE Healthcare; HASTE, Siemens Healthcare; SSH-TSE/UFSE, Philips Healthcare), which is ideal for imaging the kidneys and ureters,^{34–36} can also be used to assess the bladder in cases of severe motion artifact on conventional FSE/TSE, but generally should not be utilized for bladder staging due to the lower spatial resolution and image blur compared to conventional FSE/TSE.

DWI is now considered an integral component of bladder MRI²⁴ and in our experience improves detection of tumors compared to T₂W MRI alone (Fig. 2). Most

commercially available DWI is performed as single-shot echo-planar imaging (EPI). This sequence is very prone to artifacts especially related to susceptibility mismatches (generally from gas within adjacent bowel or metallic implants in the pelvis), which cause magnetic field inhomogeneities (that are worse at 3T), resulting in distortion and warping artifacts.³⁷ The use of a higher NEX, lower matrix size, smaller imaging field of view (FOV), parallel imaging, and fat suppression generally improves the quality of EPI and should be utilized as much as possible in bladder DWI-MRI. DWI should be performed using at least two *b* values to enable derivation of apparent diffusion coefficient (ADC) values and full ADC maps.³⁸ Typically, low *b* values (<200 sec/mm²), with or without intermediate *b* values, are combined with higher *b* value imaging performed using *b* values at least 800 sec/mm².^{39,40} It has been shown that ADC values derived from intermediate (*b* >200 sec/mm²) and high *b* values may be more representative of tumor cellularity compared to ADC values derived from DWI that includes low *b* value data (*b* <200 sec/mm²) due to a contribution from intravoxel incoherent motion or so-called “fast diffusion” at lower *b* values.⁴¹ Trace high *b* value EPI images often depict tumors as high signal intensity lesions that differ from the low signal intensity of the detrusor muscle and urine. Tumors on ADC maps are generally depicted as being of low signal (generally iso- or hypointense to the low ADC signal intensity detrusor muscle) in contrast to the high signal intensity of urine. For this reason, in our experience, the trace high *b* value EPI images often depict tumors better than ADC maps, as there is more contrast between the tumor and surrounding structures. The use of very high *b* values (>1000 sec/mm²) to improve contrast between tumor and adjacent tissues has been shown to be valuable in other pelvic tumors and is also valuable for delineating bladder tumors. Acquiring very high *b* value DWI is time-consuming, as a proportional increase in NEX is generally required to offset the loss of signal that occurs with higher diffusion weighting; however, vendors now provide commercially available software to calculate or derive the very high *b* value data by extrapolation from the lower *b* value acquisitions. Studies have shown comparable image quality in calculated high *b* value compared to acquired high *b* value DWI in the pelvis, with generally higher contrast on calculated compared to acquired images and substantial reductions in acquisition time.^{42,43} Diffusion kurtosis imaging, which models non-Gaussian diffusion effects at high *b* values, is likely useful for discriminating a posttreatment change from recurrent or residual bladder tumor,⁴⁴ and may improve bladder MRI in other ways that have yet to be explored.

Recently, several novel acquisition techniques for pelvic DWI have become commercially available and have been shown to improve image quality compared to single-shot EPI. Inhomogeneities which result in cumulative dephasing

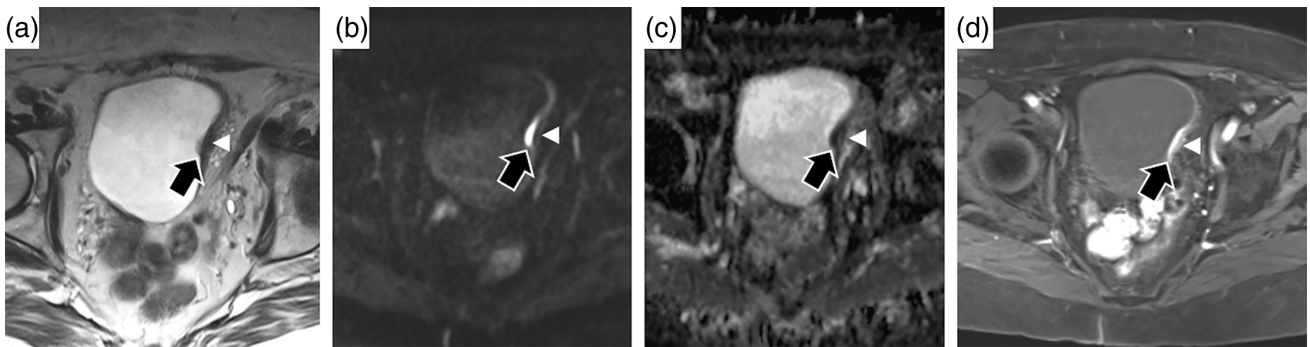


FIGURE 2: 89 year old male patient with high-grade pathological stage T1 urinary bladder cancer. **a:** Axial T_2W FSE image shows the normal low T_2W signal intensity detrusor muscle (arrowhead) with an overlying faint intermediate signal intensity intraluminal projection (arrow) representing the tumor. **b:** Axial $b = 1000 \text{ sec/mm}^2$ DWI better depicts the tumor which has very high signal intensity (arrow) compared to the low signal intensity of the detrusor muscle (arrowhead) and urine. **c:** Axial ADC map also shows the difference between the tumor (arrow) and detrusor muscle (arrowhead) with the tumor being of lower signal intensity; however, the tumor is clearly best seen on the high b value DWI. **d:** Axial image from dynamic contrast-enhanced (DCE) MRI shows the tumor is early and avidly enhancing (arrow) compared to the detrusor muscle (arrowhead). The imaging features are compatible with $<T_2$ disease.

of off-resonance spins during the EPI readout leading to mis-mapping causes spurious areas of artifactual signal increase or dropout and geometric warping and distortion on the final images.³⁷ The sensitivity of EPI to off-resonance is dependent on the rate at which k -space is sampled along the phase-encoding direction³⁷; therefore, reducing the imaging FOV along the phase-encoding direction should reduce sensitivity of EPI to susceptibility artifacts. Studies evaluating reduced FOV EPI in the pelvis (FOCUS, GE Healthcare, and Z-EPI, Siemens Healthcare) have shown improved image quality and reduced artifact compared with conventional single-shot EPI of the whole pelvis.^{37,45,46} In a case series by Rosenkrantz and Taneja, reduced FOV EPI provided diagnostic quality images in patients undergoing prostate MRI with hip prosthesis, which is otherwise generally not possible due to severe artifact encountered with conventional single-shot EPI.⁴⁷ In segmented readout EPI, the same diffusion preparation is used as in single-shot EPI; however, the k -space trajectory is divided into multiple segments in the readout direction with 2D Navigator echoes to reduce sensitivity to motion (RESOLVE, Siemens Healthcare).⁴⁸ This sampling scheme has been shown to reduce artifact and improve image quality compared to conventional k -space sampling in single-shot EPI in the pelvis.⁴⁵ Another advantage of reduced FOV DWI is higher spatial resolution compared to whole-pelvis single-shot EPI; however, smaller FOV and higher matrix sizes result in lower SNR compared to whole pelvis EPI, which requires a period of adjustment for the user and radiologists should be aware that the use of reduced FOV DWI for imaging of an organ (in this case, the bladder) results in an inability to assess the remainder of the pelvis, for example, to detect lymph node metastases.

DCE MRI is also an important component of bladder MRI.²⁴ DCE imaging is generally performed before and after gadolinium injection using fat-suppressed 3D T_1W spoiled

GRE images. Imaging planes vary; in our experience, axial or sagittal imaging is adequate in most cases. Dynamic imaging following contrast administration is essential; bladder cancers typically demonstrate enhancement on the earlier phase images (45–120 seconds after intravenous injection), along with the bladder wall mucosa, whereas the detrusor muscle appears dark on the earlier phase images and demonstrates enhancement on the more delayed images. We perform dynamic imaging every 10 seconds for 5 minutes and initiate the acquisition of images timed with the injection of gadolinium intravenously through the use of a power injector. An alternative is to perform lower temporal resolution imaging (for example, every 30 seconds) and, to our knowledge, these techniques have not been objectively compared. Lower temporal resolution would result in an ability to improve spatial resolution and coverage; however, an advantage of higher temporal resolution is the ability to extract pharmacokinetic semiquantitative and quantitative analyses (discussed below), which may be useful as future radiomic markers of bladder cancer grade and stage. The use of parallel imaging should be considered fundamental for DCE as a method to improve temporal resolution with decreases in SNR offset through the use of increased signal from gadolinium. Parallel imaging combined with keyhole imaging techniques (DISCO, GE Healthcare; TWIST, Siemens Healthcare; 4D-TRAK, Philips Healthcare) can further be implemented in the pelvis to achieve higher temporal resolution.^{49,50} More recently, the use of compressed sensing (which exploits spatial and spatio-temporal correlations) with parallel imaging has been described to accelerate acquisition times and achieve high temporal and spatial resolution.⁵¹ With compressed sensing, k -space is undersampled randomly, preferably in a radial trajectory, enabling acquisition as a free-breathing technique with robust correction of motion artifacts.⁵² In a study by Parikh et al, this technique, which employed free-breathing

continuous acquisition without a predetermined temporal resolution (which can be later reconstructed at various temporal resolutions from source data) using compressed sensing with radial acquisition (GRASP, Siemens Healthcare) achieved high-quality imaging at varying temporal resolutions during simultaneous MRU.⁵² The added value of DCE in addition to DWI and T₂W sequences for the local staging of bladder cancer is unclear, and there are limited data directly comparing the individual mp-MRI sequences.¹⁹

Concerns over nephrogenic systemic fibrosis (NSF) in patients receiving gadolinium with renal impairment (which may represent a substantial proportion of patients with bladder malignancies) have to a large part been alleviated with a markedly reduced incidence when using macrocyclic and newer linear gadolinium-based contrast agents (GBCAs).^{53,54} Nevertheless, with concerns over gadolinium deposition in the brain (which can be associated with renal impairment),^{55,56} the use of GBCA for bladder imaging should, in our opinion, be decided on a case-by-case basis. Performing nongadolinium-enhanced MRI may be a consideration for patients receiving repeated MRI exams, since the clinical effects of cumulative doses of gadolinium are unknown.

A summary of an mp-MRI technique used for imaging of the bladder is provided (Table 1). Combined imaging of the bladder and upper tracts through an MRU technique is now technically feasible on most commercial systems.³⁴ Comprehensive evaluation of the upper tracts is critical in the context of bladder cancer due to the risk of synchronous or metachronous upper tract disease.⁵⁷ CT urography (CTU) remains the preferred imaging modality, with a sensitivity of 88–100% for upper tract disease versus 69% for MRU⁵⁸; however, optimized MRU can provide an alternative for patients in which CT may be contraindicated. The sensitivity of MRU increases in the context of urinary obstruction, where CTU may be limited by poor contrast excretion into the collecting system.⁵⁸ Additionally, MRU is superior to CTU in diagnosing noncalcareous causes of urinary obstruction.⁵⁹

MRU can be performed using static-fluid sensitive and excretory techniques. Static-fluid sensitive MRU utilizes T₂W images to evaluate the collecting system and ureters (Fig. 6).³⁴ This relies on adequate distention of the urinary tract and adequate hydration is critical in nonobstructed patients. Intravenous hydration, use of a diuretic (eg, furosemide), or extrinsic compression devices may be used prior to scanning to augment ureteric filling.⁶⁰ Rapid acquisition sequential images can help distinguish fixed obstruction from ureteric peristalsis.⁶¹ Excretory MRU, on the other hand, relies on excretion of gadolinium into the collecting system where ureteric abnormalities appear as filling defects akin to CTU. The concentration of excreted gadolinium is an important consideration, as the T₂* effects of gadolinium may

overwhelm the desired T₁ shortening effect if too concentrated. This shortcoming can be overcome by utilizing diluted gadolinium (eg, reducing dose, hydrating the patient, and using a diuretic) or hepatocyte-specific gadolinium agents.³⁴

MRI Staging and Accuracy

Bladder cancer T stage is defined in the eighth edition of the American Joint Committee on Cancer (AJCC) Staging Manual.⁶² Ta refers to noninvasive papillary carcinoma and Tis refers to noninvasive carcinoma in situ or “flat tumor.” T1 bladder cancer invades the lamina propria without muscle invasion. T2 is indicated by the presence of bladder cancer muscle invasion, and can be divided into tumor limited to the inner half of the muscle (T2a) or involving the outer half of the muscle (T2b). T3 tumor invades the peri-vesical fat either microscopically (T3a) or macroscopically (T3b). T4 tumor invades the prostate, seminal vesicles, uterus, or vagina (T4a) or the pelvic or abdominal wall (T4b). Unlike prior editions, the eighth edition provides clarity on intraurethral prostatic stromal invasion, which is considered T2 disease, similar to urethral cancer staging. Tumors arising in bladder diverticula, which usually do not have a muscularis propria, can no longer be classified as T2. The eighth edition also recommends that attempts be made to subcategorize T1 disease on TURBT.

The soft-tissue contrast resolution of MRI makes it the optimal imaging exam for determining bladder cancer T stage. The manifestation of each T stage depends on the MRI sequence, with different features for T₂W images, DCE images, and DWI (Table 2). Multiple studies suggest that the accuracy of MRI for determining bladder cancer T stage is optimized when using all three of these sequences together (mp-MRI)^{17,63,64}; however, a recent meta-analysis found that there was no significant difference in accuracy of discrimination between non-MIBC and MIBC, and between the absence and presence of peri-vesical invasion, using different MRI techniques.¹⁹

On T₂W images, the normal detrusor muscle appears as a T₂ hypointense band outlining the bladder lumen.⁶⁵ An intact T₂ hypointense band suggests stage Ta, Tis, or T1 bladder cancer. An irregular inner margin at the junction of the bladder tumor and the T₂ hypointense band is considered T2a disease, while disruption of the T₂ hypointense band, without invasion of the adjacent peri-vesical fat, is considered T2b.^{66,67} Tumor signal extending into the fat is considered T3b, and extension into the adjacent organs or the pelvic wall is T4 disease.

On DCE imaging, early phase contrast-enhanced images reveal bladder tumors, the bladder mucosa, and lamina propria to enhance, whereas the underlying detrusor muscle remains hypointense, for example, between 45–120 seconds after intravenous injection.^{66,68,69} For Ta, Tis, and

TABLE 1. Sample Bladder Multiparametric MRI Protocol Performed With Pelvic Surface Coil^a at 3T^b (The Ottawa Hospital)

Sequence	Imaging plane	Field of view (mm)	Matrix size	Slice thickness/gap (mm)	TR/TE (msec)	Echo train length	Flip angle	Acceleration factor	Receiver bandwidth (Hz/voxel)	Acquisition time (min)	Number of signals averaged
T1 TSE ^c	Axial	350 x 350	320 x 320	5.0/1.0	720/ 8–14	3	111	N/A	244	4 min	2
T1 3D dual echo GRE ^d	Axial	240 x 240	292 x 224	4.0/1.0	4.8/1.1–1.3; TE12.2–2.5; TE2	N/A	12	2	558	Breath Hold	1
T2 TSE	Coronal Sagittal Axial	220 x 220	320 x 256	4.0/0 3.0/0 3.0/0	3890–5250/ 105–125	27-35	111	N/A	122	4 min 4 min 4 min	1–2
DWI ^e	Axial	280 x 280	128 x 80	3-5.0/0	4200/ 90	1	90	2	1950	5 min	4–10
T1 GRE ^f dynamic contrast	Axial	220 x 220	128 x 128	4.0/0	4.3/1.3	N/A	12	2	488	6 min	1

^aIntegrated pelvic surface coils (4–16 channels) with activated spine coils (8–12 channels).

^bClinical 3T systems: TRIO TIM (Siemens Medical, Malvern, PA) and Discovery 750W (General Electric, Milwaukee, WI).

^cTurbo/Fast Spin Echo.

^dGradient Recalled Echo.

^eDWI = Diffusion weighted imaging performed with spectral fat suppression echo planar imaging with tridirectional motion probing gradients and b values of 0, 500, 1000 with automatic apparent diffusion coefficient map generation.

^fDynamic fast spoiled 2D GRE performed with a temporal resolution of 10 seconds after injection of 0.1 mmol/kg of gadobutrol (Gadovist, Bayer, Toronto, ON) at a rate of 3 mL/sec.

TABLE 2. Bladder Cancer T Stage and Corresponding Findings for Each Multiphase MRI Sequence

Stage	Pathological description	MRI findings		
		T2W	DWI	DCE (early-phase)
Ta, Tis or T1	Ta = noninvasive papillary carcinoma, Tis = noninvasive carcinoma in situ or “flat tumor,” T1 = invasion of the lamina propria	Intermediate signal intensity tumor does not extend into the low T2W signal detrusor muscle	Flat appearing tumor, underlying thickened submucosa or a submucosal stalk that does not restrict diffusion	Muscle underlying the tumor remains hypointense, or intact submucosal linear enhancement beneath the tumor
T2	Muscle invasion into inner half of detrusor muscle (T2a) or outer half (T2b)	Irregular inner margin between tumor and low T2W signal detrusor muscle, or disruption of the low T2W signal muscle	Non-flat tumors without a submucosal component, and those that bulge with a smooth surface toward the detrusor muscle	Irregular inner margin at the junction of the tumor and muscle (T2a), or disruption of the hypointense muscle wall (T2b)
T3	Peri-vesical fat invasion microscopically (T3a) or macroscopically (T3b)	Tumor signal extends into peri-vesical fat	Irregular tumor margin toward the peri-vesical fat	Tumor enhancement extends into the peri-vesical fat
T4	Invasion of prostate, seminal vesicles, uterus or vagina (T4a), or the pelvic or abdominal wall (T4b)	Tumor signal extends into surrounding organs, pelvic or abdominal wall	Irregular tumor margin that extends into a surrounding organ, pelvic or abdominal wall	Tumor enhancement extends into surrounding organs, pelvic or abdominal wall

T2W = T2-weighted imaging, DWI = diffusion weighted imaging, DCE = dynamic contrast enhanced imaging.

T1 disease, on the early postcontrast images, the muscle underlying the tumor remains hypointense. The presence of intact submucosal linear enhancement beneath the tumor on early phase images is also indicative of Ta, Tis, or T1 disease.^{17,63} An irregular inner margin at the junction of the bladder tumor and muscle on the early postcontrast images suggests stage T2a disease, whereas disruption of the hypointense muscle wall, without early enhancing tissue extending

into the peri-vesical fat, suggests stage T2b disease (Fig. 3). T3 and T4 tumors demonstrate abnormal early enhancement extending into the peri-vesical fat and surrounding structures, respectively.

Takeuchi et al described and validated bladder cancer T stage on DWI.¹⁷ They found that flat-appearing bladder tumors, and those with either an underlying thickened submucosa or a submucosal stalk that does not restrict diffusion,

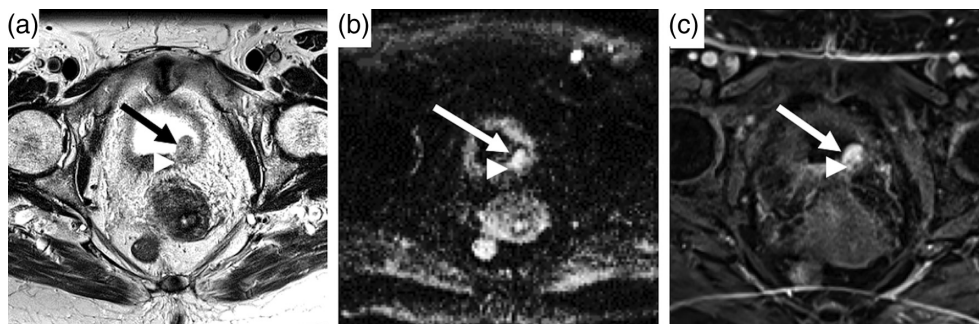


FIGURE 3: An 88-year-old female with high-grade urothelial carcinoma. T₂W image (a) shows the intermediate signal tumor (arrow) to have similar signal to the adjacent detrusor muscle (arrowhead), limiting assessment for muscle invasion. High b value DWI (b) shows the tumor (arrow) to have slightly higher signal than the bladder wall (arrowhead); however, differentiation remains difficult. c: Early DCE image shows the enhancing tumor (arrow) in contrast to the bladder wall which demonstrates relatively little enhancement. There is an irregular inner margin between the tumor and bladder wall (arrowhead), suggesting T2 disease, which was later confirmed on surgical pathology.

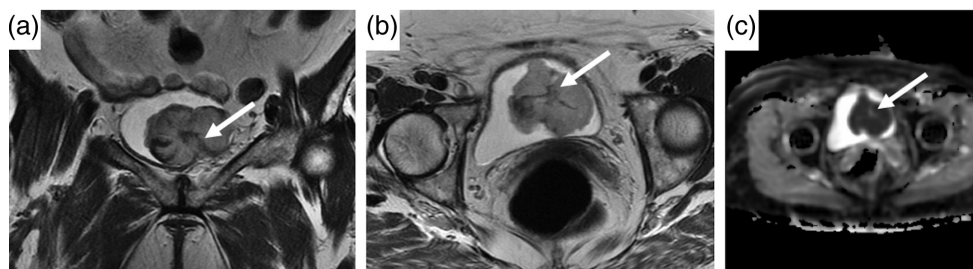


FIGURE 4: A 77-year-old female with poorly differentiated urothelial carcinoma with foci of sarcomatoid differentiation. a: Coronal T₂W image shows a mass arising from the left inferior bladder wall on a stalk (arrow). **b:** Axial T₂W image demonstrates a T2 intermediate polypoid endoluminal mass and stalk (arrow). Axial high b value ADC map demonstrates marked diffusion restriction of the mass; however, the central stalk does not demonstrate restricted diffusion (arrow), suggestive of T1 disease. pT1 bladder cancer was later confirmed on surgical pathology.

were suggestive of stage Ta, Tis, or T1 (Fig. 4). The arch-like appearance of the tumor that restricts diffusion, on thickened submucosa or a stalk that does not, was likened to the appearance of an “inchworm.” The value of a stalk for differentiating Ta, Tis, or T1 from T2 was also demonstrated by Wang et al.⁶³ Nonflat tumors without a submucosal component, and those that bulge with a smooth surface toward the muscle, are suggestive of stage T2 disease. An irregular margin toward the peri-vesical fat suggests stage T3, and if this margin extends to a surrounding organ, stage T4. Interestingly, the ADC value may also be useful for determining tumor grade. The ADC value of low-grade bladder tumors may be significantly higher than that of high-grade tumors.¹⁶

Decisions regarding treatment of bladder cancer are driven by the extent of primary tumor (ie, clinical T stage), which is determined by a combination of clinical and imaging parameters.² Clinical tests that are relied on for local staging (cystoscopy, examination under anesthesia, and TURBT) may be suboptimal.⁷⁰ Current guidelines recommend pelvic CT or MRI for local staging with the caveat that neither test is able to accurately differentiate T2 from higher-stage tumors.⁵ The most extensive clinical staging evaluation identified considerable limitations; at cystectomy, 40% of patients with clinical non-MIBC were upstaged, and 36% with clinical organ-confined disease had locally advanced disease at cystectomy.⁹

A recent systematic review and meta-analysis evaluating the accuracy of MRI for local staging of bladder cancer for four T-stage thresholds (compared to current standards for clinical staging) identified that MRI may be more accurate than originally estimated, and perhaps superior to some clinical staging strategies.¹⁹ The four thresholds evaluated were:

1. MRI to differentiate <T1 from >T2 stage before and/or after initial TURBT identifying <T1 tumor. This is critical to determine the necessity of cystectomy. Given sufficient accuracy, MRI could replace re-resection prior to intravesical therapy, lead to usage of neoadjuvant chemotherapy prior to cystectomy if muscle-

invasion is confirmed, or help guide the usage of bladder-preserving therapy with concurrent chemoradiotherapy.

2. MRI to determine T-any vs. T0 stage before and/or after initial TURBT.
3. MRI to differentiate <T2 vs. >T3 stage before and/or after initial TURBT or repeat TURBT. This can be used to help guide patients on the benefit/harm balance of neoadjuvant chemotherapy.
4. MRI to determine <T4b vs. pT4b stage, which can help determine feasibility of resection vs. palliative radiation.

The results from this meta-analysis are highlighted (Table 3). It was concluded from this study that MRI staging for <T1 vs. >T2, <T2 vs. >T3, and <T4b vs. pT4b is potentially superior to the current standard for clinical staging. However, MR accuracy for T-any vs. T0 may not be superior to clinical staging. In addition, no difference in accuracy was identified for different MR techniques (mp-MRI including DWI and DCE) for thresholds 1 and 3; there was insufficient data to evaluate technical parameters for thresholds 2 and 4. Despite the lack of difference in accuracy when comparing the addition of these individual MRI sequences to T₂W imaging, the higher accuracy of MRI than originally estimated could be due to a combination of functional imaging along with improved base resolution and higher field strength. Generalizability and clinical applicability of these results should be somewhat guarded, since there were concerns about the risk of bias of included studies (for all thresholds) and sample size (for two of the thresholds). Future prospective trials comparing clinical staging strategies vs. MR are needed.

Woo et al performed a recent meta-analysis, with a pooled sensitivity and specificity of 0.92 and 0.87, respectively, for differentiating <T1 vs. >T2 disease.²⁰ Huang et al also published a recent meta-analysis obtaining a pooled sensitivity and specificity of 0.90 and 0.88, respectively, for differentiating <T1 vs. >T2 disease.²¹

Bladder cancer N stage criteria were modified in the more recent 7th and 8th editions of the AJCC Staging

TABLE 3. Accuracy of Bladder MRI for Assessing Bladder Cancer T Stage

Study Question	Sensitivity (95% CI)	Specificity (95% CI)
Q1: Differentiate $\leq T1$ from $\geq T2$ stage before and/or after initial TURBT identifying $< T1$ tumor	87 (82–91)	79 (72–85)
Q2: Differentiate T-any vs. T0 stage before and/or after initial TURBT	65 (23–92)	90 (83–94)
Q3: Differentiate $\leq T2$ vs. $\geq T3$ stage before and/or after initial TURBT or repeat TURBT	83 (75–88)	87 (78–93)
Q4: Differentiate $< T4b$ vs. pT4b stage	85 (63–95)	98 (95–99)

Source: Gandhi et al.¹⁹ TURBT = transurethral resection of bladder tumor.

Manual.^{62,71} N stage is now determined by the number of pathologic lymph nodes, and includes common iliac nodes as regional nodal disease. N0 indicates no pathologic nodes. N1 is defined as a single regional nodal metastasis in the true pelvis, which includes the peri-vesical, obturator, internal iliac (hypogastric), external iliac, and presacral nodal stations. N2 refers to more than one nodal metastasis in the true pelvis. N3 is defined by the presence of one or more pathologic common iliac lymph nodes. Retroperitoneal lymph nodes are considered M1a disease.

Determination of pathologic lymph nodes on cross-sectional imaging is limited. This may be due to the lack of research directly correlating individual node features on imaging with node histopathology. Most studies assessing nodal disease from pelvic malignancies are on a per-patient, per-pelvic side or per-nodal station basis rather than a per-node basis.^{72–74}

Traditionally, pathologic lymph nodes were determined on cross-sectional imaging based solely on node short axis size greater than 10 mm^{26,75}; however, in 2014, Thoeny et al demonstrated that MRI could be used to detect normal-sized pathologic lymph nodes when DWI was incorporated

into the staging protocol.⁷⁴ Their approach involved first identifying lymph nodes with higher signal than inguinal nodes on DWI ($b = 1000 \text{ sec/mm}^2$). Node morphologic features were then assessed on the other sequences, with the following features considered suspicious for malignancy: round shape (equal diameter in three planes), irregular or ill-defined border, and/or lower T₂ signal than muscle or inguinal lymph nodes (Fig. 5). Nodes with eccentric fat, and symmetric pelvic nodes, were considered benign.

Node short axis size greater than 10 mm, and the approach applied by Thoeny et al above, can be used to help distinguish benign and malignant lymph nodes when staging bladder cancer.⁷⁴ Unfortunately, accuracy for determining nodal metastases on cross-sectional imaging remains limited. Despite incorporating morphologic criteria when analyzing normal size lymph nodes, Thoeny et al found that sensitivity for determining nodal metastases on a per-pelvic side basis remained limited (71% and 73%).⁷⁴

Bladder Cancer Variants

Several more aggressive histological variants of urothelial carcinoma have been described, including: plasmacytoid,

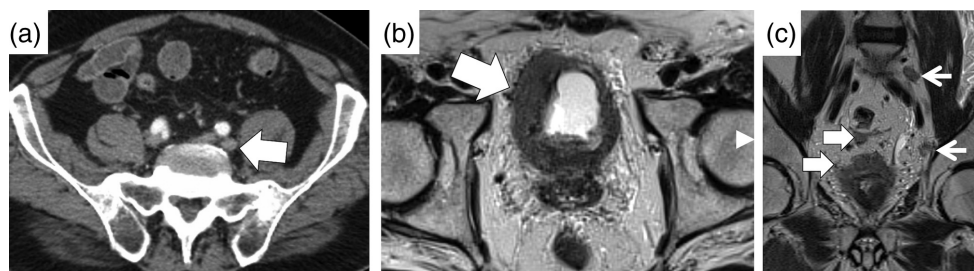


FIGURE 5: Contrast-enhanced axial CT image (a) demonstrates a left common iliac lymph node not meeting size criterion for a pathologic node (short axis >10 mm) (arrow). **b:** Axial T₂W image of the urinary bladder depicts a large mass involving predominantly the right bladder wall with extension into the peri-vesical fat (arrow). **c:** Coronal T₂W image again shows tumor extension into the peri-vesical fat (thick arrows). The normal size lymph nodes on CT were found to have abnormal morphology on MRI, namely irregular borders (thin arrows), suggestive of pathologic nodes as has been described by Thoeny et al.⁷⁴

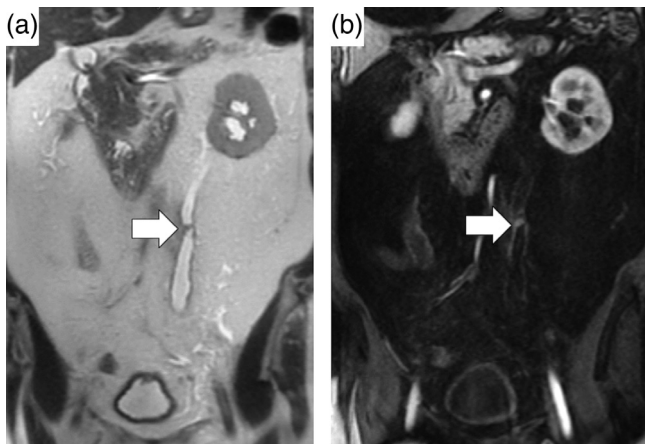


FIGURE 6: A 77-year-old female with multifocal urothelial carcinoma. **a:** Coronal T₂W image from an MR urogram demonstrates moderate left hydronephrosis with a polypoid filling defect at the level of the left mid-ureter (arrow). **b:** Coronal fat-suppressed contrast-enhanced T₁-weighted MR image in the urothelial phase demonstrates enhancement of the ureteric mass (arrow). Surgical pathology confirmed papillary urothelial carcinoma of the left ureter.

micropapillary, and sarcomatoid urothelial carcinoma.⁷⁶ Intraoperative and histopathological descriptions of plasmacytoid urothelial carcinoma (PUC) have a characteristic pattern of local invasion, with sheet-like spread of malignant cells along pelvic fascial planes.⁷⁷ This is hypothesized to be related to the loss of E-cadherin expression.⁷⁸ Recently, imaging

findings of PUC have been described resembling histological spread of tumor with invasive T₂W hypointense sheets of soft tissue extending from the primary tumor and spreading along fascial planes with restricted diffusion (Fig. 7).⁷⁹ A propensity for locally recurrent disease and peritoneal metastases has also been described in PUC.⁸⁰ Imaging features of micropapillary and sarcomatoid variants have not, to our knowledge, been described in the imaging literature.

Other epithelial neoplasms of the bladder include squamous cell and adenocarcinoma, far less common than urothelial carcinoma. Squamous cell carcinoma represents 3–7% of bladder malignancies in the United States, typically presenting in older patients.⁸¹ Common risk factors in developed nations include: neurogenic bladder and chronic bladder irritation or infection; however, schistosomiasis is a specific etiological organism associated with bladder squamous cell carcinoma, resulting in much higher rates in endemic nations.⁸² Squamous cell carcinoma demonstrates no specific imaging features, typically appearing as a focal mass or wall thickening; the exception being in the case of prior infection with schistosomiasis, where diffuse curvilinear bladder wall calcification with concomitant bladder mass should suggest a squamous cell histology.⁸³ Adenocarcinoma represents only 2% of bladder malignancies, with a third of adenocarcinomas being urachal in origin.⁸⁴ Urachal adenocarcinomas are characterized by a typical location at the midline bladder dome at

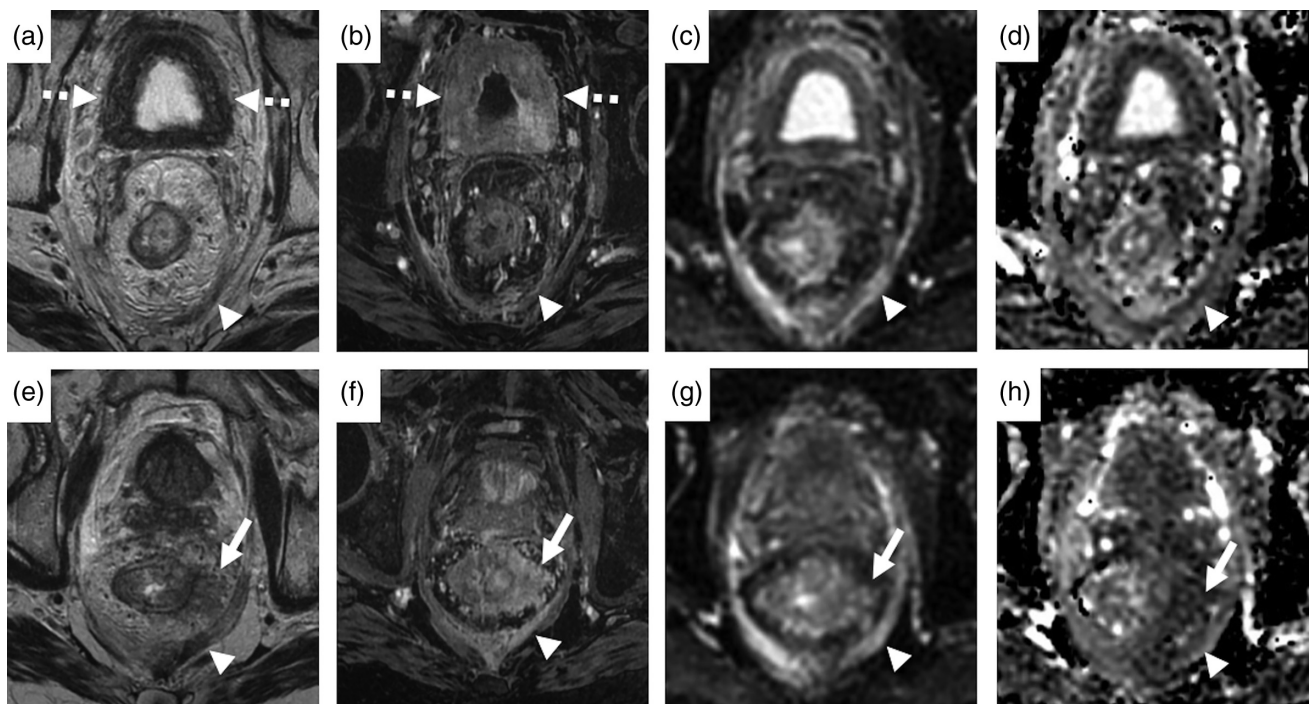


FIGURE 7: An 83-year-old male with rectal pain and biopsy-proven plasmacytoid urothelial carcinoma of the urinary bladder. Axial T₂W image **(a)** demonstrates marked bladder wall thickening (dotted arrows) and thick T₂ hypointense soft tissue extending along the mesorectal fascia (arrowhead). This soft tissue demonstrates enhancement on DCE imaging **(b)** with diffusion restriction confirmed by high signal on high b-value DWI **(c)** and low signal on the ADC map **(d)**. More confluent mass-like perirectal soft tissue is noted more inferiorly (solid white arrows), which again demonstrates low signal intensity on T₂W imaging **(e)**, with contrast enhancement **(f)** and diffusion restriction **(g,h)**. Soft tissue is again noted extending along the mesorectal fascia (arrowheads).

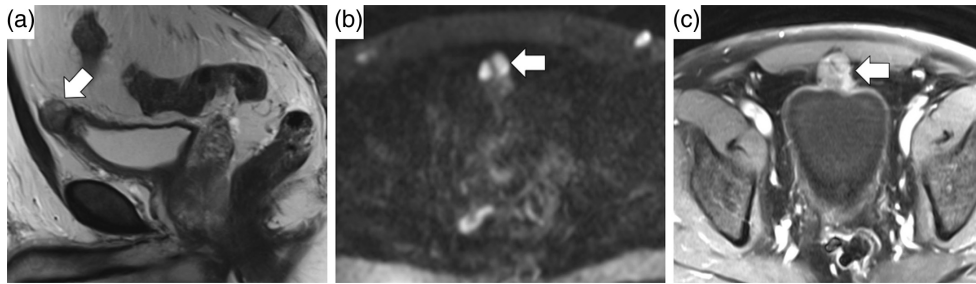


FIGURE 8: A 44-year-old male undergoing workup for gross hematuria and found to have a bladder mass on ultrasound. **a:** Sagittal T₂W image shows a mass associated with the bladder dome, at the expected location of the urachal remnant, between the dome and umbilicus (arrows). This mass restricts diffusion **(b)** and demonstrates early enhancement on DCE imaging **(c)**. Pathology revealed this mass to be a urachal adenocarcinoma.

the insertion of the median umbilical ligament (Fig. 8). Urachal adenocarcinoma mural invasion is from external to luminal, potentially resulting in a submucosal mass on imaging and at cystoscopy. Mucinous differentiation may be seen in adenocarcinomas, resulting in markedly T₂W hyperintense signal within the primary mass or nodal metastases, which may distinguish adenocarcinomas from other epithelial malignancies.⁸⁵

Malignant bladder masses may also be secondary to involvement by a nonbladder primary malignancy, either by direct invasion (eg, colonic, rectal, prostatic, or cervical carcinomas) or metastatic disease (eg, lymphoma/leukemia, gastric, melanoma, lung, or breast).⁸⁶ The remainder of bladder neoplasms are predominantly accounted for by mesenchymal tumors. These lesions are typically benign and will again preserve a smooth inner urothelial contour at imaging, suggesting their origin from the sub-urothelial layers of the bladder wall.⁸⁷

Radiomic Analysis

Radiomic analysis of mp-MRI imaging features shows promise at both predicting local tumor stage and histological grade of bladder cancer.^{88–90} T₂W images can be used to evaluate tumor heterogeneity, which is a marker for various

histological features (including cellular proliferation, necrosis, tumor angiogenesis) and can be evaluated quantitatively using texture analysis.^{88,91} Radiomic features can be extracted from functional MRI images providing information on tumor biology at the cellular level. For example, ADC analysis provides information regarding the diffusivity of water, which is influenced by tumor cellularity, cell membrane integrity, and structural changes.^{90,92} Diffusion kurtosis imaging may have a relationship with the complexity of microstructures in tissues.⁴⁴ DCE analysis can further provide information regarding tumor microvasculature and surrounding cellular environment.⁹³

Several quantitative features may be useful for predicting tumor stage prior to surgery in addition to qualitative visual assessment of the primary tumor, bladder wall, and surrounding fat on T₂W, DWI, and DCE imaging.^{88,89} A few T₂W textural features can help differentiate normal bladder wall from cancer,^{93,94} and certain radiomic textural features may be associated with MIBC.⁸⁸ Whether texture analysis is useful for diagnosis of >T2 disease remains unknown and requires further study. In addition to tumor stage, radiomic features have been found to provide information on tumor grade and disease aggressiveness, factors that impact both medical and surgical management.^{93,95–97} DCE-derived tumor washout may be associated with higher-grade cancer⁹³

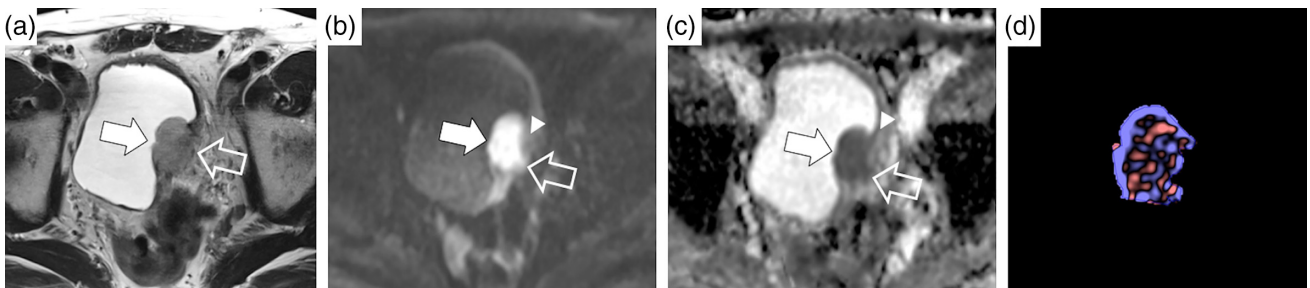


FIGURE 9: A 63-year-old male with high-grade T3 bladder urothelial carcinoma. Lobulated urothelial carcinoma (solid white arrows) arising from the left bladder wall with intermediate signal on the axial T₂W image **(a)**, marked restricted diffusion with high signal on the $b = 1000 \text{ sec/mm}^2$ **(b)** and corresponding low signal on the ADC map **(c)**. Intermediate T₂ signal intensity and corresponding restricted diffusion (open arrows) extends from the tumor, through the bladder wall (arrowheads), and into the peri-vesical fat, consistent with T3b disease. The tumor was contoured using commercially available texture analysis software and the corresponding entropy texture map **(d)** visually demonstrates the textural data. Preliminary data shows promise in certain textural features being able to predict stage and grade of tumor. Further work is needed prior to widespread clinical use.

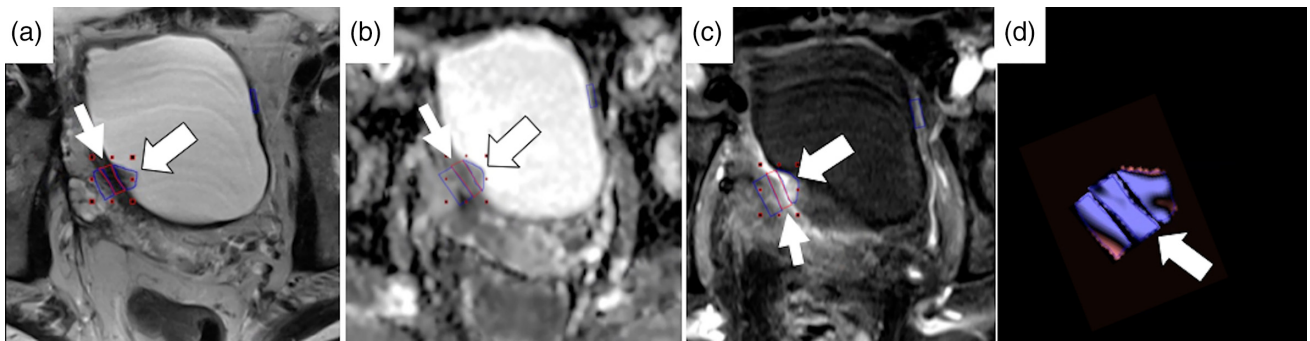


FIGURE 10: A 69-year-old male with low-grade T1 bladder cancer. A lobulated mass (large white arrow) arising from the right bladder wall with intermediate T₂W signal on the axial T₂W image (a) and marked restricted diffusion with low signal on the ADC map (b). The mass demonstrates enhancement on early DCE imaging (c). The adjacent bladder wall (small white arrow) has been contoured for texture analysis on T₂W imaging, ADC map, and DCE imaging using commercially available texture analysis software. The corresponding texture map (d) visually demonstrates the textural data, showing the tumor to be more homogeneous than the tumor in Fig. 9.

and quantitative ADC values have been shown to inversely correlate with tumor grade.⁹² Combining ADC values with different texture features (including entropy and kurtosis) shows promise for predicting higher-grade bladder cancer, although further work is needed to verify the results from these preliminary studies.^{90,93} Examples illustrating radiomic texture analysis of urinary bladder tumors are depicted for both relatively more heterogeneous (Fig. 9) and homogeneous (Fig. 10) tumors.

There are several common genetic mutations associated with bladder cancer, including those affecting cell-cycle regulation, chromatin regulation, and kinase signaling pathways.⁹⁸ Known distinct genetic pathways between MIBC and non-MIBC may often account for the differences in clinical outcomes and patient prognosis.^{26,99} Non-MIBC are associated with mutations involving fibroblastic growth factors, which affects the kinase signaling pathways, while MIBC can be associated with defects in p53 and retinoblastoma tumor suppressor pathways, which affect cell cycle control.^{99,100} Knowledge of these pathways may be helpful for the discovery of useful radiomic features associated with different genetic mutations.^{38,100} A study by Sevcenco et al showed an association between ADC values and cell cycle regulators including p53 and p21.¹⁰⁰ Also Ki-67, which is a known marker for cellular proliferation, has been shown to inversely correlate with ADC values.¹⁰¹ These findings suggest that features on ADC may be useful biomarkers in the radiomic analysis of bladder cancer. As knowledge of the genetic basis of bladder tumors evolves and the application of radiomic features derived from MRI improves, the potential for MRI biomarkers to become a noninvasive diagnostic test useful for assessing the genetic makeup of tumors, providing more accurate grading and staging of disease, may be realized.

A recent and rapidly expanding area of study in medical imaging is the application of deep learning (ie, artificial intelligence) to imaging data. This includes algorithms that have incorporated radiomic features for bladder cancer staging and

assessment of treatment response.^{102,103} Work on machine-learning models that can automatically detect and segment organs and disease processes in the abdomen and pelvis is under way. Future research directions may include automated detection of bladder tumors, bladder tumor subtype differentiation, and the development of prediction models for bladder tumors likely to respond to treatment.

Conclusion

The future contribution of MRI to the management of bladder cancer will likely increase as the accuracy of MRI compared to current staging techniques is more widely recognized, particularly with regard to identification of muscle invasion. The application of radiomic features, and incorporation of machine-learning algorithms to enhance interpretation of bladder MRI, may further improve staging accuracy and may also provide other useful information such as assessment of treatment response. Current bladder cancer management guidelines may benefit from further integration of MRI into their staging strategies. Moving forward, studies are needed to assess the added value of mp-MRI for the preoperative grading and staging of urinary bladder cancer using traditional and emerging MRI techniques, and to further explore bladder cancer radiomic analysis and the application of machine learning to bladder cancer MRI.

References

1. American Cancer Society. Cancer Statistics Center: Urinary Bladder at a Glance. Available at: <https://www.cancer.org/cancer/bladder-cancer.html>. Accessed May 12, 2018.
2. McInnes MD, Siemens DR, Mackillop WJ, et al. Utilisation of preoperative imaging for muscle-invasive bladder cancer: a population-based study. *BJU Int* 2016;117:430–438.
3. Expert Panel on Urologic Imaging: van der Pol CB, Sahni VA, et al. ACR appropriateness criteria®: pretreatment staging of muscle-invasive bladder cancer. *J Am Coll Radiol* 2018;15:S150–S159.
4. Nayak B, Dogra PN, Naswa N, Kumar R. Diuretic 18F-FDG PET/CT imaging for detection and locoregional staging of urinary bladder

- cancer: prospective evaluation of a novel technique. *Eur J Nucl Med Mol Imaging* 2013;40:386–393.
5. National Comprehensive Cancer Network (NCCN). Clinical Practice Guidelines in Oncology (NCCN Guidelines®): Bladder Cancer (Version 3.2018). Available at: https://www.nccn.org/professionals/physician_gls/PDF/bladder.pdf. Accessed April 12, 2018.
 6. Chang SS, Boorjian SA, Chou R, et al. Diagnosis and treatment of non-muscle invasive bladder cancer: AUA/SUO Guideline. *J Urol* 2016;196:1021–1029.
 7. Babjuk M, Bohle A, Burger M, et al. EAU guidelines on non-muscle-invasive urothelial carcinoma of the bladder: update 2016. *Eur Urol* 2017;71:447–461.
 8. Richards KA, Smith ND, Steinberg GD. The importance of transurethral resection of bladder tumor in the management of nonmuscle invasive bladder cancer: a systematic review of novel technologies. *J Urol* 2014;191:1655–1664.
 9. Shariat SF, Palapattu GS, Karakiewicz PI, et al. Discrepancy between clinical and pathologic stage: impact on prognosis after radical cystectomy. *Eur Urol* 2007;51:137–149; discussion 149–151.
 10. Dutta SC, Smith JA Jr, Shappell SB, Coffey CS, Chang SS, Cookson MS. Clinical under staging of high risk nonmuscle invasive urothelial carcinoma treated with radical cystectomy. *J Urol* 2001;166:490–493.
 11. Hollenbeck BK, Ye Z, Dunn RL, Montie JE, Birkmeyer JD. Provider treatment intensity and outcomes for patients with early-stage bladder cancer. *J Natl Cancer Inst* 2009;101:571–580.
 12. Rabie E, Faeghi F, Izadpanahi MH, Dayani MA. Role of dynamic contrast-enhanced magnetic resonance imaging in staging of bladder cancer. *J Clin Diagn Res* 2016;10:Tc01–05.
 13. Daneshmand S, Ahmadi H, Huynh LN, Dobos N. Preoperative staging of invasive bladder cancer with dynamic gadolinium-enhanced magnetic resonance imaging: results from a prospective study. *Urology* 2012;80:1313–1318.
 14. Rajesh A, Sokhi HK, Fung R, Mulcahy KA, Bankart MJ. Bladder cancer: evaluation of staging accuracy using dynamic MRI. *Clin Radiol* 2011;66:1140–1145.
 15. Gupta N, Sureka B, Kumar MM, Malik A, Bhushan TB, Mohanty NK. Comparison of dynamic contrast-enhanced and diffusion weighted magnetic resonance image in staging and grading of carcinoma bladder with histopathological correlation. *Urol Ann* 2015;7:199–204.
 16. Wang HJ, Pui MH, Guo Y, et al. Multiparametric 3-T MRI for differentiating low-versus high-grade and category T1 versus T2 bladder urothelial carcinoma. *AJR Am J Roentgenol* 2015;204:330–334.
 17. Takeuchi M, Sasaki S, Ito M, et al. Urinary bladder cancer: diffusion-weighted MR imaging—accuracy for diagnosing T stage and estimating histologic grade. *Radiology* 2009;251:112–121.
 18. van der Pol CB, Shinagare AB, Tirumani SH, Preston MA, Vangel MG, Silverman SG. Bladder cancer local staging: multiparametric MRI performance following transurethral resection. *Abdom Radiol (NY)* 2018 [Epub ahead of print].
 19. Gandhi N, Krishna S, Booth CM, et al. Diagnostic accuracy of MRI for tumor staging of bladder cancer: Systematic review and Meta-Analysis. *BJU Int* 2018 [Epub ahead of print].
 20. Woo S, Suh CH, Kim SY, Cho JY, Kim SH. Diagnostic performance of MRI for prediction of muscle-invasiveness of bladder cancer: A systematic review and meta-analysis. *Eur J Radiol* 2017;95:46–55.
 21. Huang L, Kong Q, Liu Z, Wang J, Kang Z, Zhu Y. The diagnostic value of MR imaging in differentiating T staging of bladder cancer: a meta-analysis. *Radiology* 2018;286:502–511.
 22. Petersen R, Sesterhenn I, Davis C. Chapter 3: Urinary bladder In: *Urologic pathology*. Philadelphia: Lippincott Williams & Wilkins; 2009.
 23. Tanagho E, Lue T. Chapter 1: Anatomy of the genitourinary tract. In: *Smith & Tanagho's general urology*. New York: McGraw-Hill; 2013.
 24. de Haas RJ, Steyvers MJ, Futterer JJ. Multiparametric MRI of the bladder: ready for clinical routine? *AJR Am J Roentgenol* 2014;202:1187–1195.
 25. Narumi Y, Kadota T, Inoue E, et al. Bladder wall morphology: in vitro MR imaging-histopathologic correlation. *Radiology* 1993;187:151–155.
 26. Verma S, Rajesh A, Prasad SR, et al. Urinary bladder cancer: role of MR imaging. *Radiographics* 2012;32:371–387.
 27. Hecht EM, Yitta S, Lim RP, et al. Preliminary clinical experience at 3 T with a 3D T2-weighted sequence compared with multiplanar 2D for evaluation of the female pelvis. *AJR Am J Roentgenol* 2011;197:W346–352.
 28. Kim H, Lim JS, Choi JY, et al. Rectal cancer: comparison of accuracy of local-regional staging with two- and three-dimensional preoperative 3-T MR imaging. *Radiology* 2010;254:485–492.
 29. Proscia N, Jaffe TA, Neville AM, Wang CL, Dale BM, Merkle EM. MRI of the pelvis in women: 3D versus 2D T2-weighted technique. *AJR Am J Roentgenol* 2010;195:254–259.
 30. Wagner M, Rief M, Busch J, et al. Effect of butylscopolamine on image quality in MRI of the prostate. *Clin Radiol* 2010;65:460–464.
 31. Fujimoto K, Koyama T, Tamai K, Morisawa N, Okada T, Togashi K. BLADE acquisition method improves T2-weighted MR images of the female pelvis compared with a standard fast spin-echo sequence. *Eur J Radiol* 2011;80:796–801.
 32. Lane BF, Vandermeer FQ, Oz RC, Irwin EW, McMillan AB, Wong-You-Cheong JJ. Comparison of sagittal T2-weighted BLADE and fast spin-echo MRI of the female pelvis for motion artifact and lesion detection. *AJR Am J Roentgenol* 2011;197:W307–313.
 33. Froehlich J, Metens T, Chilla B, Hauser N, Klarhoefer M, Kubik-Huch R. Should less motion sensitive T2-weighted BLADE TSE replace Cartesian TSE for female pelvic MRI? *Insights Imaging* 2012;3:611–618.
 34. Chung AD, Schieda N, Shanbhogue AK, Dilauro M, Rosenkrantz AB, Siegelman ES. MRI evaluation of the urothelial tract: pitfalls and solutions. *AJR Am J Roentgenol* 2016;W108–W116.
 35. Krishna S, Schieda N, Flood TA, Shanbhogue AK, Ramanathan S, Siegelman E. Magnetic resonance imaging (MRI) of the renal sinus. *Abdom Radiol (NY)* 2018 [Epub ahead of print].
 36. Ramamurthy NK, Moosavi B, McInnes MD, Flood TA, Schieda N. Multiparametric MRI of solid renal masses: pearls and pitfalls. *Clin Radiol* 2015;70:304–316.
 37. Warndahl BA, Borisch EA, Kawashima A, Riederer SJ, Froemming AT. Conventional vs. reduced field of view diffusion weighted imaging of the prostate: Comparison of image quality, correlation with histology, and inter-reader agreement. *Magn Reson Imaging* 2018;47:67–76.
 38. Qayyum A. Diffusion-weighted imaging in the abdomen and pelvis: concepts and applications. *Radiographics* 2009;29:1797–1810.
 39. Yoshida S, Takahara T, Kwee TC, Waseda Y, Kobayashi S, Fujii Y. DWI as an imaging biomarker for bladder cancer. *AJR Am J Roentgenol* 2017:1–11.
 40. Padhani AR, Liu G, Koh DM, et al. Diffusion-weighted magnetic resonance imaging as a cancer biomarker: consensus and recommendations. *Neoplasia* 2009;11:102–125.
 41. Takahara T, Kwee TC. Low b-value diffusion-weighted imaging: emerging applications in the body. *J Magn Reson Imaging* 2012;35:1266–1273.
 42. Maas MC, Futterer JJ, Scheenen TW. Quantitative evaluation of computed high B value diffusion-weighted magnetic resonance imaging of the prostate. *Invest Radiol* 2013;48:779–786.
 43. Grant KB, Agarwal HK, Shih JH, et al. Comparison of calculated and acquired high b value diffusion-weighted imaging in prostate cancer. *Abdom Imaging* 2015;40:578–586.
 44. Wang F, Jin D, Hua XL, et al. Investigation of diffusion kurtosis imaging for discriminating tumors from inflammatory lesions after treatment for bladder cancer. *J Magn Reson Imaging* 2018;48:259–265.
 45. Attenberger UI, Rathmann N, Sertdemir M, et al. Small field-of-view single-shot EPI-DWI of the prostate: Evaluation of spatially-tailored two-dimensional radiofrequency excitation pulses. *Z Med Phys* 2016;26:168–176.

46. Brendle C, Martirosian P, Schwenzer NF, et al. Diffusion-weighted imaging in the assessment of prostate cancer: Comparison of zoomed imaging and conventional technique. *Eur J Radiol* 2016;85:893–900.
47. Rosenkrantz AB, Taneja SS. Use of reduced field-of-view acquisition to improve prostate cancer visualization on diffusion-weighted magnetic resonance imaging in the presence of hip implants: report of 2 cases. *Curr Probl Diagn Radiol* 2018;47:125–127.
48. Li L, Wang L, Deng M, et al. Feasibility study of 3-T DWI of the prostate: readout-segmented versus single-shot echo-planar imaging. *AJR Am J Roentgenol* 2015;205:70–76.
49. Othman AE, Martirosian P, Schraml C, et al. Feasibility of CAIPIRINHA-Dixon-TWIST-VIBE for dynamic contrast-enhanced MRI of the prostate. *Eur J Radiol* 2015;84:2110–2116.
50. Saranathan M, Rettmann DW, Hargreaves BA, Clarke SE, Vasanawala SS. Differential subsampling with Cartesian ordering (DISCO): a high spatio-temporal resolution Dixon imaging sequence for multiphase contrast enhanced abdominal imaging. *J Magn Reson Imaging* 2012;35:1484–1492.
51. Rosenkrantz AB, Geppert C, Grimm R, et al. Dynamic contrast-enhanced MRI of the prostate with high spatiotemporal resolution using compressed sensing, parallel imaging, and continuous golden-angle radial sampling: preliminary experience. *J Magn Reson Imaging* 2015;41:1365–1373.
52. Parikh N, Ream JM, Zhang HC, Block KT, Chandarana H, Rosenkrantz AB. Performance of simultaneous high temporal resolution quantitative perfusion imaging of bladder tumors and conventional multi-phase urography using a novel free-breathing continuously acquired radial compressed-sensing MRI sequence. *Magn Reson Imaging* 2016;34:694–698.
53. Martin DR, Krishnamoorthy SK, Kalb B, et al. Decreased incidence of NSF in patients on dialysis after changing gadolinium contrast-enhanced MRI protocols. *J Magn Reson Imaging* 2010;31:440–446.
54. Edward M, Quinn JA, Burden AD, Newton BB, Jardine AG. Effect of different classes of gadolinium-based contrast agents on control and nephrogenic systemic fibrosis-derived fibroblast proliferation. *Radiology* 2010;256:735–743.
55. Kanda T, Ishii K, Kawaguchi H, Kitajima K, Takenaka D. High signal intensity in the dentate nucleus and globus pallidus on unenhanced T1-weighted MR images: relationship with increasing cumulative dose of a gadolinium-based contrast material. *Radiology* 2014;270:834–841.
56. Cao Y, Zhang Y, Shih G, et al. Effect of renal function on gadolinium-related signal increases on unenhanced T1-weighted brain magnetic resonance imaging. *Invest Radiol* 2016;51:677–682.
57. Yousem DM, Gatewood OM, Goldman SM, Marshall FF. Synchronous and metachronous transitional cell carcinoma of the urinary tract: prevalence, incidence, and radiographic detection. *Radiology* 1988;167:613–618.
58. Razavi SA, Sadigh G, Kelly AM, Cronin P. Comparative effectiveness of imaging modalities for the diagnosis of upper and lower urinary tract malignancy: a critically appraised topic. *Acad Radiol* 2012;19:1134–1140.
59. Shokeir AA, El-Diasty T, Eassa W, et al. Diagnosis of noncalcareous hydronephrosis: role of magnetic resonance urography and noncontrast computed tomography. *Urology* 2004;63:225–229.
60. Rothpearl A, Frager D, Subramanian A, et al. MR urography: technique and application. *Radiology* 1995;194:125–130.
61. Leyendecker JR, Barnes CE, Zagoria RJ. MR urography: techniques and clinical applications. *Radiographics* 2008;28:23–46; discussion 46–27.
62. Amin M, Edge S, Greene F, et al. *AJCC Cancer Staging Manual, 8th Edition*. New York: Springer; 2017.
63. Wang HJ, Pui MH, Guan J, et al. Comparison of early submucosal enhancement and tumor stalk in staging bladder urothelial carcinoma. *AJR Am J Roentgenol* 2016;1–7.
64. Panebianco V, De Berardinis E, Barchetti G, et al. An evaluation of morphological and functional multi-parametric MRI sequences in classifying non-muscle and muscle invasive bladder cancer. *Eur Radiol* 2017;27:3759–3766.
65. Vikram R, Ng CS, Tamboli P, et al. Papillary renal cell carcinoma: radiologic-pathologic correlation and spectrum of disease. *Radiographics* 2009;29:741–754; discussion 755–747.
66. Tekes A, Kamel I, Imam K, et al. Dynamic MRI of bladder cancer: evaluation of staging accuracy. *AJR Am J Roentgenol* 2005;184:121–127.
67. Kim B, Semelka RC, Ascher SM, Chalpin DB, Carroll PR, Hricak H. Bladder tumor staging: comparison of contrast-enhanced CT, T1- and T2-weighted MR imaging, dynamic gadolinium-enhanced imaging, and late gadolinium-enhanced imaging. *Radiology* 1994;193:239–245.
68. Neuerburg JM, Bohndorf K, Sohn M, Teufel F, Guenther RW, Daus HJ. Urinary bladder neoplasms: evaluation with contrast-enhanced MR imaging. *Radiology* 1989;172:739–743.
69. Tanimoto A, Yuasa Y, Imai Y, et al. Bladder tumor staging: comparison of conventional and gadolinium-enhanced dynamic MR imaging and CT. *Radiology* 1992;185:741–747.
70. Bellmunt J, Orsola A, Leow JJ, Wiegell T, De Santis M, Horwich A. Bladder cancer: ESMO Practice Guidelines for diagnosis, treatment and follow-up. *Ann Oncol* 2014;25(Suppl 3):iii40–48.
71. Edge S, Byrd DR, Compton CC, Fritz AG, Greene FL, Trotti A. *AJCC Cancer Staging Manual, 7th Edition*: New York: Springer; 2010.
72. Papalia R, Simone G, Grasso R, et al. Diffusion-weighted magnetic resonance imaging in patients selected for radical cystectomy: detection rate of pelvic lymph node metastases. *BJU Int* 2012;109:1031–1036.
73. Kim JK, Kim KA, Park BW, Kim N, Cho KS. Feasibility of diffusion-weighted imaging in the differentiation of metastatic from nonmetastatic lymph nodes: early experience. *J Magn Reson Imaging* 2008;28:714–719.
74. Thoeny HC, Froehlich JM, Triantafyllou M, et al. Metastases in normal-sized pelvic lymph nodes: detection with diffusion-weighted MR imaging. *Radiology* 2014;273:125–135.
75. McMahon CJ, Rofsky NM, Pedrosa I. Lymphatic metastases from pelvic tumors: anatomic classification, characterization, and staging. *Radiology* 2010;254:31–46.
76. Kassouf W, Traboulsi SL, Kulkarni GS, et al. CUA guidelines on the management of non-muscle invasive bladder cancer. *Can Urol Assoc J* 2015;9:E690–704.
77. Kaimakliotis HZ, Monn MF, Cheng L, et al. Plasmacytoid bladder cancer: variant histology with aggressive behavior and a new mode of invasion along fascial planes. *Urology* 2014;83:1112–1116.
78. Lim MG, Adsay NV, Grignon DJ, Osunkoya AO. E-cadherin expression in plasmacytoid, signet ring cell and micropapillary variants of urothelial carcinoma: comparison with usual-type high-grade urothelial carcinoma. *Mod Pathol* 2011;24:241–247.
79. Chung AD, Schieda N, Flood TA, et al. Plasmacytoid urothelial carcinoma (PUC): Imaging features with histopathological correlation. *Can Urol Assoc J* 2017;11:E50–E57.
80. Dayyani F, Czerniak BA, Sircar K, et al. Plasmacytoid urothelial carcinoma, a chemosensitive cancer with poor prognosis, and peritoneal carcinomatosis. *J Urol* 2013;189:1656–1661.
81. Wong JT, Wasserman NF, Padurean AM. Bladder squamous cell carcinoma. *Radiographics* 2004;24:855–860.
82. Martin JW, Carballido EM, Ahmed A, et al. Squamous cell carcinoma of the urinary bladder: Systematic review of clinical characteristics and therapeutic approaches. *Arab J Urol* 2016;14:183–191.
83. Poturalski MJ, Magi-Galluzzi C, Liu PS. Squamous cell carcinoma of the bladder complicating schistosomiasis: AIRP best cases in radiologic-pathologic correlation. *Radiographics* 2017;37:500–504.
84. Wong-You-Cheong JJ, Woodward PJ, Manning MA, Sesterhenn IA. From the archives of the AFIP: neoplasms of the urinary bladder: radiologic-pathologic correlation. *Radiographics* 2006;26:553–580.

85. Chung AD, Schieda N, Flood TA, et al. Suburothelial and extrinsic lesions of the urinary bladder: radiologic and pathologic features with emphasis on MR imaging. *Abdom Imaging* 2015;40:2573–2588.
86. Bates AW, Baithun SI. Secondary neoplasms of the bladder are histological mimics of nontransitional cell primary tumours: clinicopathological and histological features of 282 cases. *Histopathology* 2000;36:32–40.
87. Chen M, Lipson SA, Hricak H. MR imaging evaluation of benign mesenchymal tumors of the urinary bladder. *AJR Am J Roentgenol* 1997;168:399–403.
88. Xu X, Liu Y, Zhang X, et al. Preoperative prediction of muscular invasiveness of bladder cancer with radiomic features on conventional MRI and its high-order derivative maps. *Abdom Radiol (NY)* 2017;42:1896–1905.
89. Zhang X, Xu X, Tian Q, et al. Radiomics assessment of bladder cancer grade using texture features from diffusion-weighted imaging. *J Magn Reson Imaging* 2017;46:1281–1288.
90. Rosenkrantz AB, Obele C, Rusinek H, et al. Whole-lesion diffusion metrics for assessment of bladder cancer aggressiveness. *Abdom Imaging* 2015;40:327–332.
91. Hanahan D, Weinberg RA. The hallmarks of cancer. *Cell* 2000;100:57–70.
92. Kobayashi S, Koga F, Yoshida S, et al. Diagnostic performance of diffusion-weighted magnetic resonance imaging in bladder cancer: potential utility of apparent diffusion coefficient values as a biomarker to predict clinical aggressiveness. *Eur Radiol* 2011;21:2178–2186.
93. Zhou G, Chen X, Zhang J, Zhu J, Zong G, Wang Z. Contrast-enhanced dynamic and diffusion-weighted MR imaging at 3.0T to assess aggressiveness of bladder cancer. *Eur J Radiol* 2014;83:2013–2018.
94. Shi Z, Yang Z, Zhang G, et al. Characterization of texture features of bladder carcinoma and the bladder wall on MRI: initial experience. *Acad Radiol* 2013;20:930–938.
95. Xu X, Zhang X, Tian Q, et al. Three-dimensional texture features from intensity and high-order derivative maps for the discrimination between bladder tumors and wall tissues via MRI. *Int J Comput Assist Radiol Surg* 2017;12:645–656.
96. Mammen S, Krishna S, Quon M, et al. Diagnostic accuracy of qualitative and quantitative computed tomography analysis for diagnosis of pathological grade and stage in upper tract urothelial cell carcinoma. *J Comput Assist Tomogr* 2018;42:204–210.
97. Zhang GM, Sun H, Shi B, Jin ZY, Xue HD. Quantitative CT texture analysis for evaluating histologic grade of urothelial carcinoma. *Abdom Radiol (NY)* 2017;42:561–568.
98. Cancer Genome Atlas Research N. Comprehensive molecular characterization of urothelial bladder carcinoma. *Nature* 2014;507:315–322.
99. Wu XR. Urothelial tumorigenesis: a tale of divergent pathways. *Nat Rev Cancer* 2005;5:713–725.
100. Sevcenco S, Haitel A, Ponhold L, et al. Quantitative apparent diffusion coefficient measurements obtained by 3-Tesla MRI are correlated with biomarkers of bladder cancer proliferative activity. *PLoS One* 2014;9:e106866.
101. Kobayashi S, Koga F, Kajino K, et al. Apparent diffusion coefficient value reflects invasive and proliferative potential of bladder cancer. *J Magn Reson Imaging* 2014;39:172–178.
102. Garapati SS, Hadjiiski L, Cha KH, et al. Urinary bladder cancer staging in CT urography using machine learning. *Med Phys* 2017;44:5814–5823.
103. Cha KH, Hadjiiski L, Chan HP, et al. Bladder cancer treatment response assessment in CT using radiomics with deep-learning. *Sci Rep* 2017;7:8738.